

Instantaneous Core Loss – Cycle-by-cycle Modeling of Power Magnetics in PWM DC/AC Converters

Binyu Cui, Jun Wang
University of Bristol

Abstract— Nowadays, PWM excitation is one of the most common waveforms seen by magnetic components in power electronic converters. Core loss modelling approaches such as improved Generalized Steinmetz equation (iGSE) or the loss map based on composite waveform hypothesis (CWH) generally process the PWM excitation piecewisely, which is proven to be effective for DC/DC converters. As the additional challenge in DC/AC converters, the fundamental-frequency sinewave component induces the ‘major loop loss’ on top of the piecewise high-frequency segments, which however cannot be modelled on a switching cycle basis by any existing methods. To address this gap, this paper proposes a novel fundamental concept, instantaneous core loss, which is observed empirically for the first time in history. Enabled by the reactive voltage cancellation method, the instantaneous core loss that only contains the real power loss can be measured as a function of time. Following this concept, a modelling method is proposed to break down the major loop core loss, typically an average value in the literature, into the time domain to enable a cycle-by-cycle modelling as a practical workflow for predicting core losses in PWM converters. Through experiments, the existence of the major loop loss is verified, and generic instantaneous core loss models are extracted for several magnetic materials/components. An example workflow of is proposed to extract the cycle-by-cycle core loss at the design stage of a PWM DC/AC converter. This work enhances the fundamental understanding of the core loss process in real time as a scientific contribution.

Index Terms—Core loss, Instantaneous loss measurement, Loss map, Magnetic

I. INTRODUCTION

Magnetic components are installed in almost all modern power electronic converters, and their power loss significantly impacts the system performance. However, there are no satisfactory first-principal models to capture all core loss mechanisms, especially under an arbitrary excitation waveform, due to the magnetic material’s non-linear property and other intricate factors such as geometries. With the advancement of wide-bandgap power semiconductor devices (e.g. Silicon Carbide) and circuit topologies, a higher switching frequency appears in more high-performance power converters as a trend, which calls for a better co-optimization with the passive components. Accurate loss modelling becomes increasingly important in these applications to correctly size the thermal management system, especially for the critical magnetic components, e.g. inductors and transformers. Despite the past research on core loss modeling under arbitrary

waveforms, the prediction and understanding of core loss in magnetic components under PWM excitations remains challenging [1-4], especially in DC/AC converters with a varying duty cycle and fundamental components in every switching cycle. The most common modelling method used in the industry is the Steinmetz equation (SE) and its variants [5][6].

$$\overline{P}_v = k f^\alpha B^\beta \quad (1)$$

These models are empirical equations that rely on curve fitting to acquire the Steinmetz parameter under a certain frequency range. The original SE is only applicable to sinusoidal waveforms whereas a modified version of SE, the improved Generalized Steinmetz equation (iGSE), is introduced to extend it to arbitrary waveforms.

$$P = \frac{1}{T} \int_0^T k \left| \frac{dB}{dt} \right|^\alpha (B_{pk})^{\beta-\alpha} dt \quad (2)$$

Although its accuracy is limited by the original SE parameters, the iGSE is typically applied by considering any arbitrary waveform as a series of piecewise linear segments, calculating the total core loss by summing the losses from each segment, which is known as the composite waveform hypothesis (CWH). CWH has been validated in previous works providing an intuitive understanding of the core loss mechanisms [7-9], of which the basic application scenario is DC/DC converters with fixed duty cycles.

One application example of CWH in DC/AC converters is the loss map method proposed in [8][10][11][12] which utilizes a pre-measured look-up table that contains the core loss of a magnetic component under different operating conditions to model the overall core loss under PWM excitations. This method calculates the total core loss under the PWM excitations by adding up the ‘major loop loss’ and the ‘minor loop loss’, which represent the fundamental frequency and switching frequency component respectively. The concept of major and minor loops comes from the B-H trajectory of the magnetic component in the scale of the switching cycle and fundamental cycle. Fig. 1 presents an example of the B-H trajectory under the sinusoidal PWM (SPWM) excitation. The figure shows an extreme case where the frequency modulation ratio (f_{sw}/f_0) is 4 to better illustrate the relationship between major and minor loops in one fundamental cycle. For the minor loop loss, one of the key challenges is the unclosed B-H loop caused by the asymmetric voltage/duty cycle applied in one switching cycle as shown in Fig. 2. An unclosed cycle contains the real core loss power together with the reactive power during the magnetizing and demagnetizing process. To extract the loss from the

unclosed minor loop, the CWH is followed as proposed in [6] by treating the minor loop as two pieces each of which can be seen as half of one completed B-H loop to be looked up in the loss map under the ‘half loop assumption’ – such a half loop is associated with 50% of the loss found in the corresponding symmetric full loop.

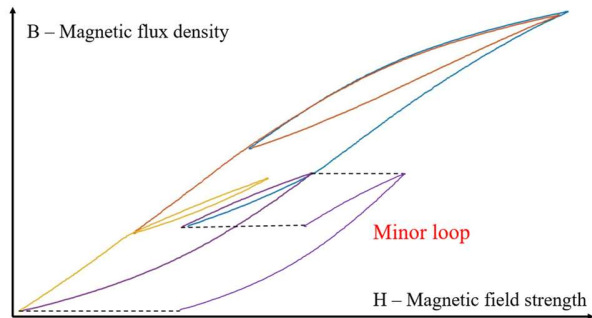


Fig. 1. One minor loop in the SPWM B-H trajectory.

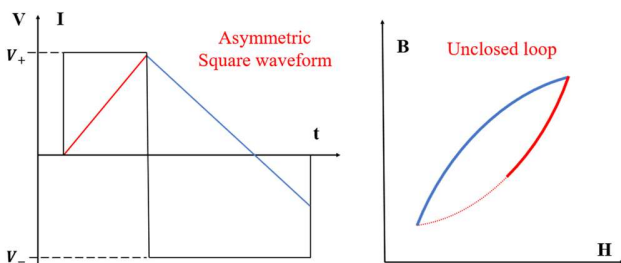


Fig. 2. Asymmetrical waveform and corresponding unclosed B-H trajectory.

However, CWH shows its limitation in the analysis of the major loop loss in DC/AC converters as it can only be applied in the scope of one switching cycle. The definition of the major loop is unclear throughout different research papers. There are papers defining the loops from its visual trajectory [13] [14] and other papers tend to calculate the loss directly from the sinusoidal excitation based on the fundamental and switching frequency of the PWM excitation [10][11]. Regardless of how the major loop is defined and extracted, its associated loss can only be found when a fundamental cycle is completed and the whole BH trajectory is closed in the existing approaches. This means the major loop loss can only be seen/modelled as an average value over one fundamental cycle. However, from the physics point of view, the core loss, encompassing both hysteresis and eddy current losses, should be dissipated instantaneously and continuously at any point on the BH trajectory rather than a sudden burst at the end of a fundamental cycle [15]. Therefore, there is a gap in the current theories/approaches towards instantaneous and cycle-by-cycle modelling of core loss.

Hence, this paper proposes a novel fundamental concept, the **instantaneous core loss**, which is an extension/application of the definition of real and reactive power by Steinmetz [16] and the Instantaneous Power Theory by Akagi [17] in the context of core loss. The introduced instantaneous core loss can be observed through the reactive cancellation method [18][19] where the real power loss can be extracted from the apparent power waveform by adding a reference air core in the testing circuit to

cancel out the reactive power. The compensated voltage is in phase with the current waveform which leads to the instantaneous core loss (real power) in the tested component being measured as a real-time signal. By applying this method in the loss map modelling, the restraint of characterizing the core loss instantaneously can be resolved. Moreover, the application of this approach can serve as a supplement to the composite waveform hypothesis for DC/AC converters. The contributions of this paper are as follows.

- 1) The major/minor loop modelling approach under PWM excitation is revisited and verified. A demonstration of how major loop loss contributes to total loss under different frequency conditions is provided.
- 2) The instantaneous core loss is empirically observed, by applying the reactive cancellation method, and defined as a concept for the first time.
- 3) Based on the measured data, normalized instantaneous loss generic model is proposed, which represents the time-domain behaviour of a magnetic component.
- 4) A practical workflow is proposed to extract the cycle-by-cycle low-frequency/major-loop loss to complete the loss map approach for practical design and modelling purposes.

The remainder of this paper is structured as follows. Section II outlines the methodology for extracting both major and minor loop losses and discusses the limitations of the previously established definition of major loop loss. Section III details the reactive cancellation approach used to obtain the instantaneous core loss, along with experimental validation. It also introduces the concept of an instantaneous loss generic model based on the previously acquired data. Section IV presents the complete workflow for applying the reactive cancellation approach to derive instantaneous core loss from scratch. Section V highlights the potential applications of this approach and its profound implications for future fundamental research on core loss. Finally, Section VI concludes the paper.

II. MAJOR AND MINOR LOOP LOSS ANALYSIS

As mentioned in the previous section, the major and minor loop loss calculation has been used to evaluate the core loss under PWM excitation. However, most research studies are lack of focus on the major loop loss which is the low-frequency loss component in the PWM excitation. In the previous studies, the major loop loss is calculated through the equivalent sinusoidal excitation loss with the same frequency. This is caused by the inadequacy in the definition of major loop loss, and it will introduce inaccuracy to the modelling. This section uses SPWM as the excitation to interpret the relationship between major and minor loop loss. Before exploring the limitation of the definition, the methodology of extracting the major loop loss and minor loop loss is first introduced here.

For one minor loop in the B-H trajectory under general SPWM excitation in one fundamental cycle, asymmetric quasi-square-wave excitation is the most common condition to be witnessed as shown in Fig. 2. As mentioned earlier, CWH is adopted to consider the asymmetric waveform piecewisely. The core idea of this method is to decompose an arbitrary PWM

waveform into half-loop segments with a constant polarity of dB/dt. Each decomposed segment as shown in Fig. 3 contributes the loss which is equivalent to half of the total loss of a closed B-H loop with the applied magnetic flux density, magnetic field strength and frequency.

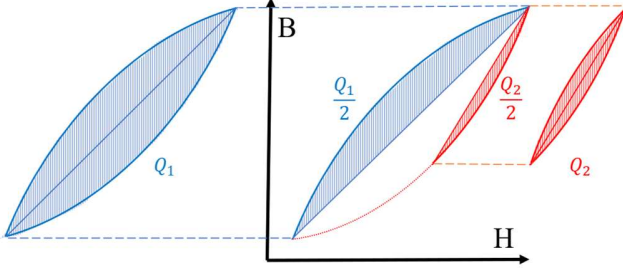


Fig. 3. CWH concept in B-H domain.

As it has been outlined in [20], three assumptions are followed in this approach.

- 1) The start and end points of one half-loop segment are defined by the turning point of the trajectory where the dB/dt changes its polarity.
- 2) For a B-H loop under symmetrical square waveform excitation, the positive half and the negative half both contribute 50% of the total energy loss.
- 3) ‘Relaxation effect’ is not considered in this situation since the general inverter topologies won’t experience any constant flux density.

For the minor loop in the PWM excitation, there are two general asymmetric conditions that can be separated by the magnetizing and demagnetizing process in the fundamental cycle as shown in Fig. 4 and Fig. 5 respectively.

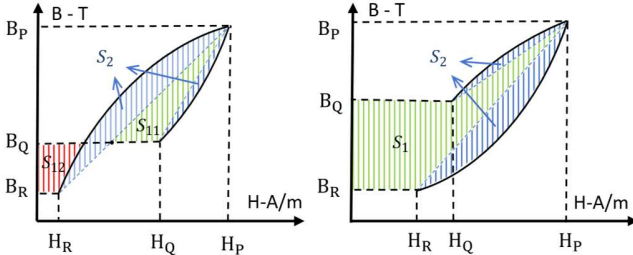


Fig. 4. Demagnetizing process.

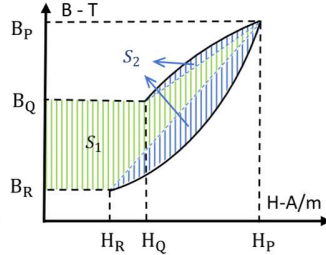


Fig. 5. Magnetizing process.

The blue-shaded area, S2, represents the core losses associated with the B-H loop trajectory from Q to P and R. They are known as the minor loop loss which can be calculated by the CWH. The green-shaded area, S1, is the reactive power across the filter inductor in one fundamental cycle. The stored and generated energy of the inductor during the magnetizing and demagnetizing process can be expressed as,

$$P_{mj_demag} = \int_{B_Q}^{B_P} H dB - \int_{B_P}^{B_R} H dB = S_{11} - S_{12} \quad (3)$$

$$P_{mj_mag} = \int_{B_Q}^{B_P} H dB - \int_{B_P}^{B_R} H dB = S_1 \quad (4)$$

Since the core loss is considered to be instantaneous loss, the major loop loss of one fundamental cycle can be expressed as (6) where k is the frequency index ratio.

$$P_{mj_loss} = \sum_{n=k/2} P_{mj_mag} + \sum_{n=k/2} P_{mj_demag} \quad (5)$$

Another way to extract the major loop loss is to consider the frequency domain. When the filter inductor is driven by an SPWM excitation, its current can be decomposed via Fourier transformation into low-frequency components associated with the fundamental frequency and high-frequency components related to the switching frequency. The derivation for each frequency component of the current can be expressed as:

$$i_L(t) = i_{hf} + i_{Lf} \quad (6)$$

$$i_{Lf} = \sum_{n=1}^{n=k} \{a_n \cos(n\omega t) + b_n \cos(n\omega t)\} \quad (7)$$

$$i_{hf} = \sum_{n=k}^{n=N} \{a_n \cos(n\omega t) + b_n \cos(n\omega t)\} \quad (8)$$

where k equals the range that can cover the low-frequency component as indicated in [10]. Fig. 6. presents an example demonstrating the proportion of the major and minor losses relative to the total core loss of the magnetic component under SPWM excitation. To isolate the inductive characteristics, the tested component is driven by a full bridge switching configuration without any load attached. The circuit parameters and magnetic component parameters are provided in Tables I and II respectively.

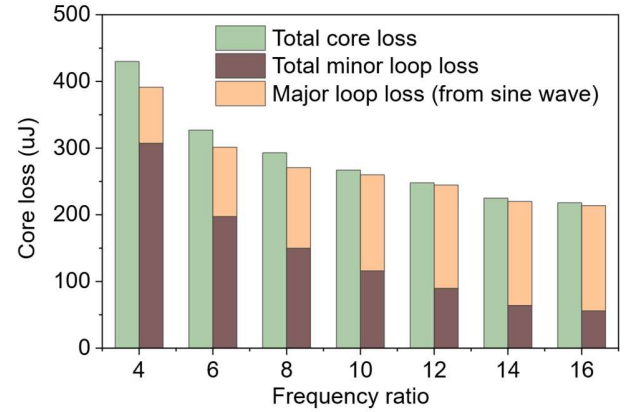


Fig. 6. Major and minor loop loss proportions against different frequency ratio.

TABLE I
TEST CIRCUIT PARAMETER

Design Parameter	Value
Input voltage	20V
Fundamental frequency	2.5kHz
Frequency index ratio	4-16
Output inductance	264uH

TABLE II
PARAMETER OF INDUCTOR UNDER TEST

Inductor parameter	Value
Core material	N87
Core shape	Toroidal

Effective length	255.3mm
Effective area	267.2mm ²
Primary winding turn	9
Secondary winding turn	9

Unlike typical SPWM applications, this test aims to reduce the ratio to its minimum value in order to evaluate the limitations of the proposed major and minor loop modelling. The experiment is conducted on a full-bridge switching circuit, with voltage and current acquired via a two-winding measurement approach. The total minor loop loss is determined by applying the CWH method to a database generated by the ATPT setup [21], while the major loop loss is derived from the lower-frequency components extracted from the current waveform. Fig. 7 and Fig. 8 present the proportions of major loop loss (unshaded area) and minor loop loss (shaded area) within the B-H loop under frequency ratios of 4 and 16, respectively. In the extreme case of a frequency ratio of 4, the minor loop loss occupies a large portion of the total loss, and a 10% discrepancy arises between the total core loss and the sum of the major and minor loop losses. As the frequency ratio increases, the major loop loss constitutes a larger fraction of the total loss, and the error rate decreases to below 1% at a ratio of 16.

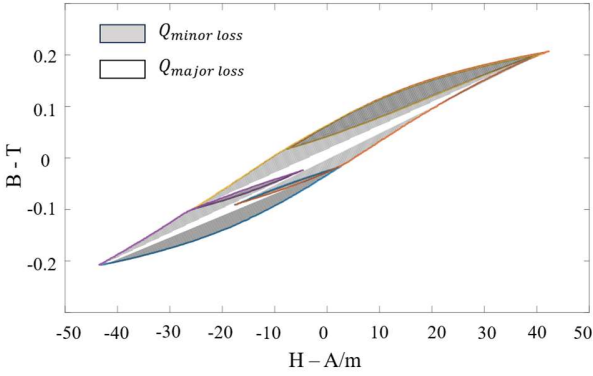


Fig. 7. Major & minor loss distribution under frequency ratio = 4.

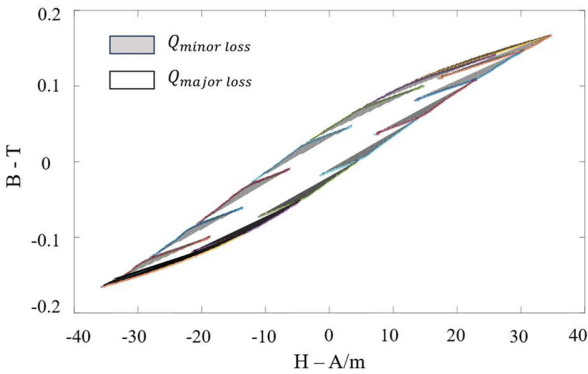


Fig. 8. Major & minor loss distribution under frequency ratio = 16.

The reason for this issue is shown in Fig. 9 where the output of the fast Fourier transforms of inductor current under frequency ratio equals 4 and 16 are illustrated. Although the fundamental frequency remains unchanged, the amplitude of the 2.5 kHz component at a ratio of 4 is reduced by 18% compared to that at a ratio of 16. This reduction occurs because the 10 kHz component is too close to the 2.5 kHz component, causing

dispersion of the main frequency component into higher-order harmonics. As a result, some major loop loss is not captured during testing. The test result outlines two important conclusions for the later proposed modelling

- 1) For a pure inductive load under excitation that contains a dominant frequency component, the major loop loss is crucial to loss modelling as it contributes a considerable fraction of the total core loss.
- 2) Under the low-frequency ratio index, the major and minor loop modelling is not feasible due to the switching frequency lying on the higher harmonic in the frequency domain. However, the method shows promising results under general operating conditions.

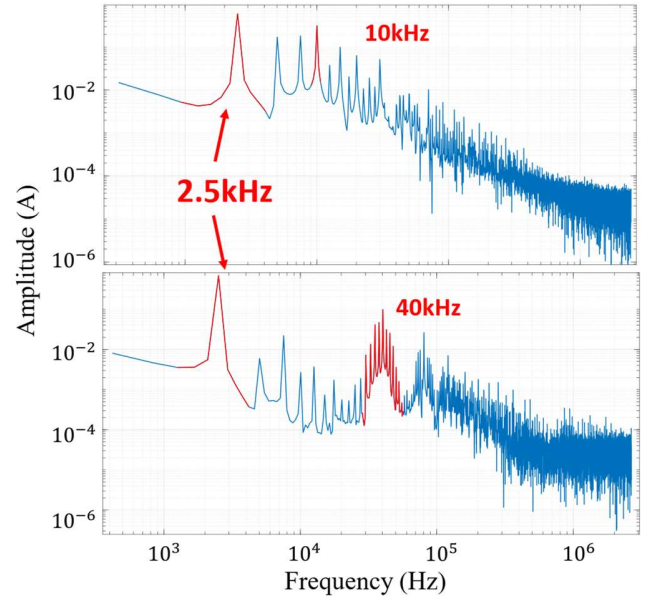


Fig. 9. FFT results at frequency ratio = 4 & frequency ratio = 16.

Following the existing approach in [10], Fig. 10 shows the cycle-by-cycle loss caused by the low-frequency and high-frequency components respectively when the frequency ratio is 16. Switching index indicates the order of the sixteen switching cycles within the fundamental cycle. Each switching cycle has a corresponding major and minor loop loss. The minor loop loss, derived via the CWH method, remains positive at all times. In contrast, the major loop loss is extracted from a sinusoidal excitation whose values will vary between positive and negative as it involves reactive power during the calculation. It can be seen that the approach in [10] results in negative major loop loss values, which inaccurately represent the instantaneous loss caused by a low-frequency component. The modelling method using major and minor loops can only be carried out at the fundamental cycle level due to the limitation of the major loop loss modelling. In the next section, a modified method is proposed that could model the instantaneous major loop loss. This approach can act as a supplement to the loss map method when modelling magnetic components under complicated modulation excitation. It also helps the CWH to take the major loop loss into consideration at the level of the switching cycle.

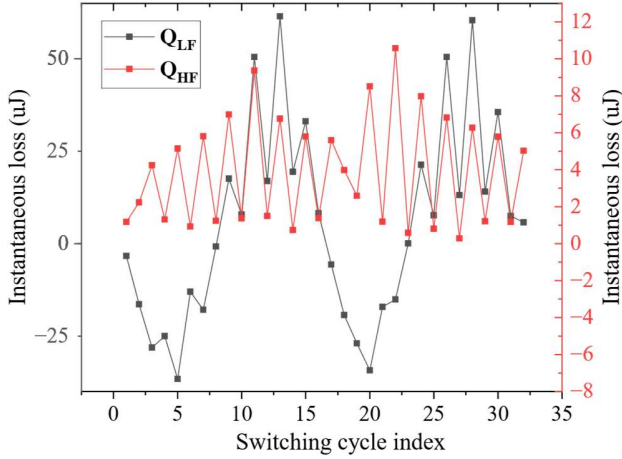


Fig. 10. Cycle-by-cycle major & minor loop loss under 2.5kHz & 40kHz SPWM excitation applying the approach in [10]

III. INSTANTANEOUS CORE LOSS

The proposed method in this section was originally used to eliminate phase discrepancies in the measurement [18] [19], but it can also provide an in-phase voltage waveform that excludes the inductor's reactive power. The key principle of this setup is to place a reference air-based inductor with the same inductance value in series with the inductor under test. As shown in Fig. 11, R_C represents the core loss generated by the inductor under tested and the L_m is the inductance of both inductors. If the turn ratio of $N1:N2$ and $N3:N4$ both equals to 1, and the inductors maintain the same inductance under any arbitrary excitation, the voltage output can be derived as:

$$V_{out} = (j\omega L_{m1} - j\omega L_{m2} - R_C)I_{pri} \quad (9)$$

With the $L_{m1} = L_{m2}$, the inductive components cancel out, leaving the output voltage directly related to the equivalent loss resistor. Consequently, the voltage waveform aligns in phase with the primary current, allowing the instantaneous loss to be determined. It should be noted that inductance matching must be performed under the specific test waveform, as inductance may vary with different excitation conditions. Under these considerations, the core loss can be expressed as:

$$P_{loss} = \frac{1}{T} \int_0^T I_{pri} V_{out} dt \quad (10)$$

A. Experimental measurement of instantaneous core loss

The magnetic component under test is a two-winding toroidal iron powder core [22] with a winding ratio of 1:1. A reference air core with identical inductance is connected in series with the component under test. Experiments are first carried out under sinusoidal excitation to guarantee the cancellation. The detailed specifications of the two cores are listed in Table III.

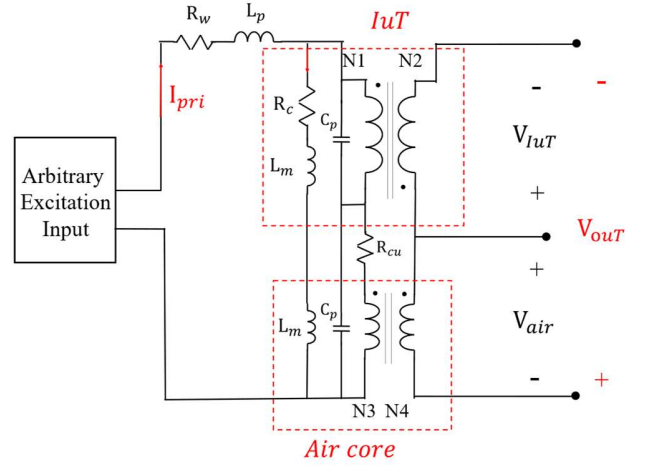


Fig. 11. Schematic of the reactive cancellation approach.



Fig. 12 Air core transformer.

TABLE III
PARAMETER OF AIR CORE AND POWDER CORE

Core Parameter	Value
Air core S_e	$467.6cm^2$
Air core l_e	14.2cm
Air core turns	23:23
T300-26D turns	28:28

For a 5kHz sinusoidal excitation applied to the load, the resulting waveform acquired from the oscilloscope is shown in Fig. 13. The V_{sec} and V_{air} exhibited nearly identical amplitudes with negligible phase shifts. The resulting voltage, V_{out} , shows a general trend of sinusoidal waveform with some fluctuation on both positive and negative sides. By integrating the V_{out} and I_{pri} , the instantaneous power of one full cycle is illustrated in Fig. 14. It can be seen that the loss dissipated in the charging stage of the inductor is relatively higher than during the discharging stage. **Explain.** This characteristic is further confirmed on N87 material which is shown in Fig. 15. The instantaneous loss shows a similar loss trend in the charging/discharging state.

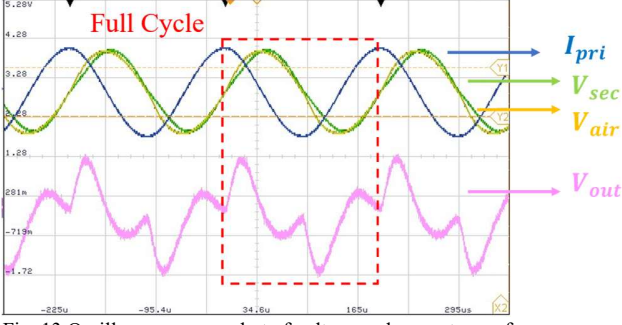


Fig. 13 Oscilloscope screenshot of voltage and current waveform.

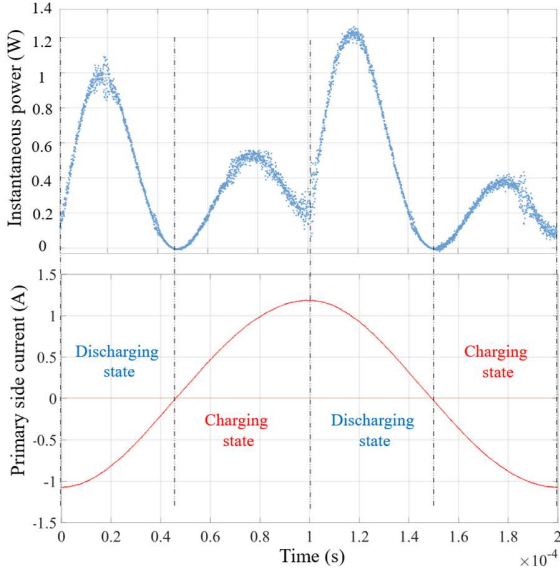


Fig. 14. T300-26D loss distribution against current waveform.

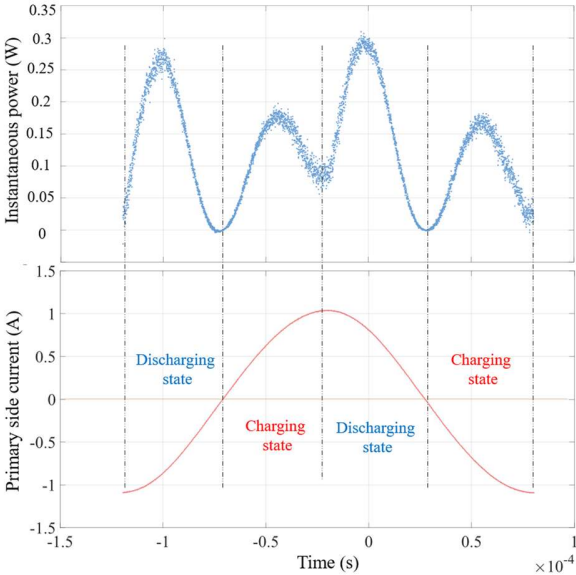


Fig. 15. N87 loss distribution against current waveform.

Fig.16 and 17 present the instantaneous core loss distributions for T300-26D and N87 within the B–H domain. Unlike conventional approaches that determine core loss only after

completing a full fundamental cycle, this method enables the extraction of instantaneous loss at any point without closing the B–H trajectory. Moreover, the accuracy of the proposed approach is verified by comparing the total loss obtained from the inductor’s measured voltage and current with the loss derived using V_{out} . These results, summarized in Table IV, show a difference of only 4%. The instantaneous loss for each half of the B–H loop is also evaluated, indicating that the loss difference between the positive and negative half-cycles is less than 3%. This outcome confirms the accuracy of the CWH method, where one key assumption states that the positive and negative half-loops contribute equally to the total core loss of a closed B–H loop.

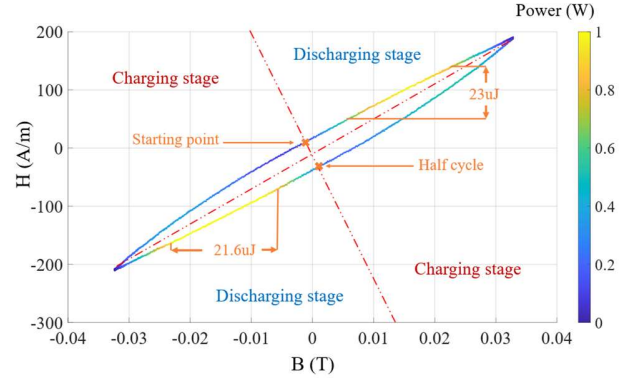


Fig. 16. T300-26D loss distribution in B-H domain.

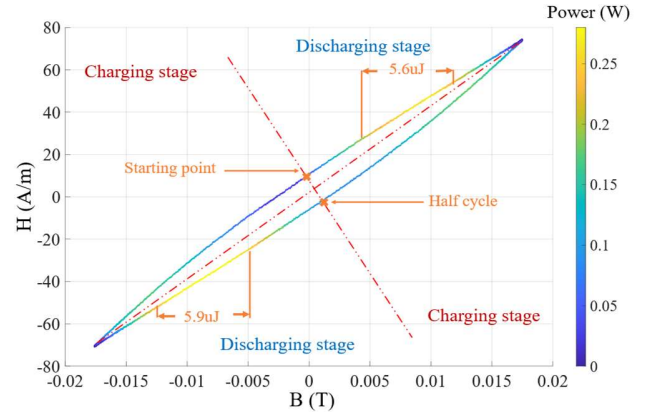


Fig. 17. N87 loss distribution in B-H domain.

TABLE IV
LOSS RESULT COMPARISON

Core material	N87	T300-26D
Actual loss (uJ)	24.9	85.2
Calculated loss (uJ)	26.1	85.7
Positive half-loop loss (uJ)	12.4	36.9
Negative half-loop loss (uJ)	13.7	38.8

B. Instantaneous core loss generic model

With the capability to evaluate loss at any instantaneous point within a single cycle, the proposed method allows direct

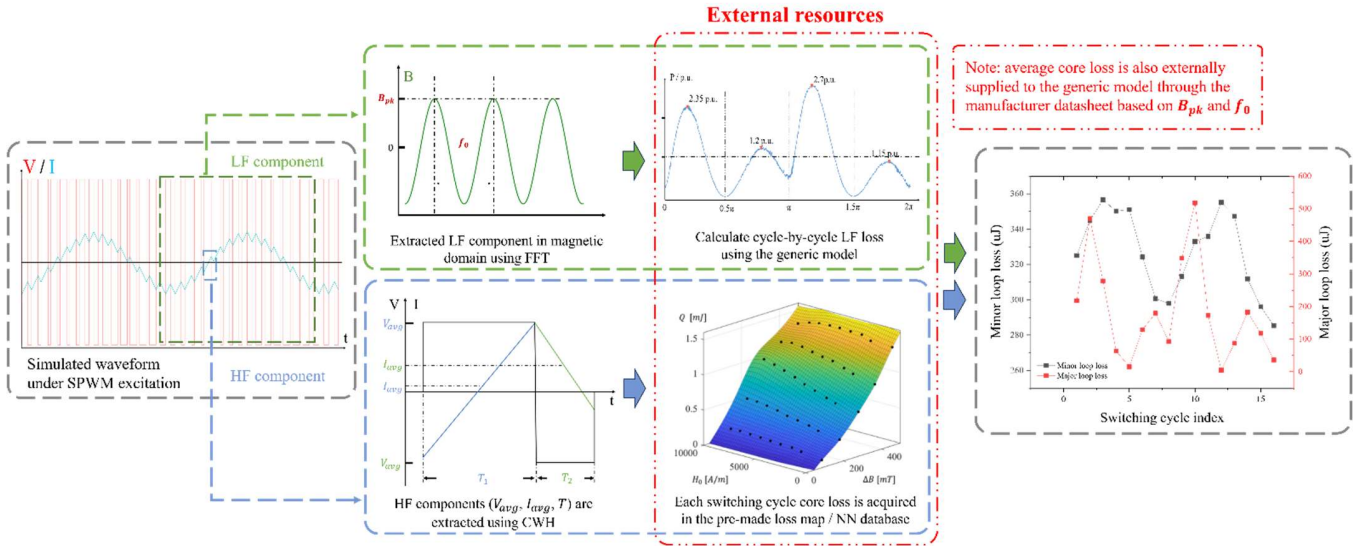


Fig. 20. Practical instantaneous core loss acquisition workflow

extraction of low-frequency losses in each switching cycle under PWM excitation. The original CWH approach can be modified by adding the cycle-by-cycle low-frequency component loss to each switching cycle while adding up the piecewise high-frequency component loss. This could be applied to the loss map method where the loss map of sinusoidal excitation can be added and extracted in the look-up table instead of calculating the total major loop loss after one fundamental cycle is closed. To achieve practical applicability, a material-based mapping model is required for determining the loss at arbitrary operating points. Use T300-26D as an example, loss distributions of multiple operation points with different frequency and voltage amplitude are demonstrated in Fig. 18.

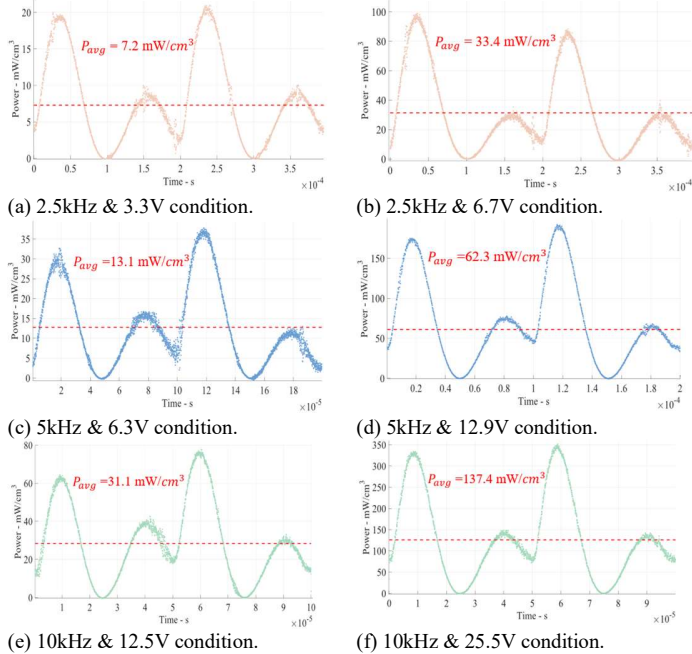


Fig. 18. Instantaneous core loss distribution under different operating conditions.

The distribution shows a similar pattern across the frequency range and flux density range where the charging state generated more loss than the discharging state and the core loss value matches between the B-H half cycle. Using the average power as the unit base, a normalized loss distribution can be acquired from each data point. Thus, a generic model shown in Fig.19 can be concluded using (11). To enable fast and accurate estimation at any given data point, the distribution pattern can be curve-fitted into a Fourier series (12) with a coefficient of determination higher than 0.99 and the associated parameters are demonstrated in the appendix Table V. It should be noted that the generic model proposed in this section is considered as component based due to the different characteristics caused by the geometry and material.

$$P_{normalized} = \frac{P_{actual}}{P_{avg}} \quad (11)$$

$$P(t) = a_0 + \sum_{n=1}^6 a_n \cos(nwt) + b_n \sin(nwt) \quad (12)$$

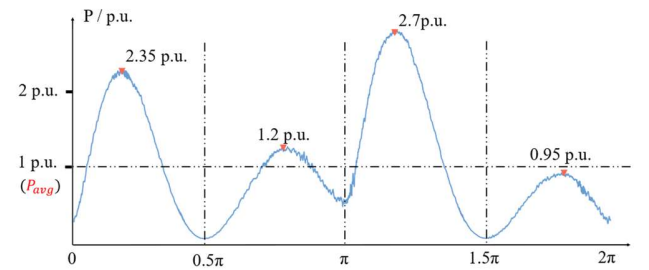


Fig. 19. Normalized instantaneous loss distribution.

IV. CYCLE-BY-CYCLE CORE LOSS MODELLING

In the practical inductor design scenario, the generic loss model can be applied in combination with the manufacture datasheet to provide a rapid and accurate calculation of the core loss value in time series. The workflow of utilizing the normalized instantaneous model in the DC/AC inverter design is demonstrated in Fig. 20 and as follows. In this scenario, an SPWM excitation with the specification indicated in Table V is applied to a T300-26D testing core. In order to determine the

instantaneous core loss, the low-frequency component and the high-frequency component have to be separated and analyzed individually. For the low-frequency component in the PWM waveform, FFT is used to extract the fundamental-frequency-based sinusoidal component from the excitation waveform. Using the frequency and the magnetic flux peak value of the extracted sinusoidal component, the average core loss can be located by the method (13) provided by the manufacturer datasheet [22] which in this case is 109.3 mW/cm^3 .

$$P_{avg} (\text{mW/cm}^3) = \frac{f}{\frac{a}{B_{pk}^3} + \frac{b}{B_{pk}^3} + \frac{c}{B_{pk}^3}} + d * B_{pk}^2 * f^2 \quad (13)$$

TABLE V
TESTING PARAMETER

Electrical Parameter	Value
Input voltage	35V
Fundamental frequency	2.5kHz
Frequency index ratio	16
Output inductance	105uH

By applying the average core loss to the generic model shown in Fig. 19, the cycle-by-cycle low-frequency core loss is derived from the modulation distribution across the fundamental cycle, as illustrated in Fig. 21. For the high-frequency component, CWM is applied to the asymmetric waveform of each switching cycle to extract positive and negative half cycles in a piecewise manner. Using the pre-measured loss map plotted via ATPT [21], along with the loss map coordinates ($V * T$, V_{pk} , I_0) of each half cycle, the corresponding high-frequency loss of each switching cycle can be determined. The cycle-by-cycle losses for both the low- and high-frequency (LF & HF) components are presented in Fig. 22, while the detailed loss values at each stage are listed in Table 6. It can be seen that the HF loss distribution has two peaks across the cycle which shows a similar trend as reported in [23] while the LF loss distribution shows the trend of the generic model.

V. OUTLOOK

The proposed concept of instantaneous core loss provides a novel perspective to enhance the fundamental understanding of core loss in the time domain, moving beyond conventional approaches that only consider the average power loss of a full period. Considering the trend of applying neural networks to model power magnetics [24][25], this work is expected to enable further development of these data-driven approaches for the time-domain modeling of core behaviour, e.g. predicting $H(t)$ from $B(t)$. Moreover, the proposed measurement approach is expected to enhance the research on physics-based modeling of core losses [26][27], e.g. as an empirical benchmark for verification or time-domain representation of the behaviours. Furthermore, in high-power industrial scenarios, this work enables a more precise modeling of the thermal cycles of power magnetics which can facilitate improved thermal management and yield more robust component designs.

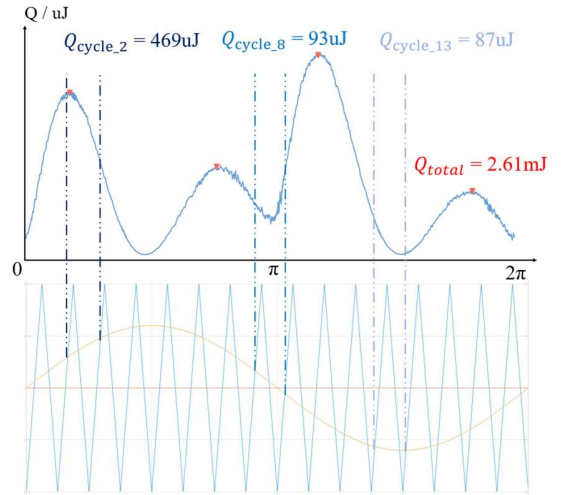


Fig. 21. Cycle-by-cycle loss distribution of SPWM excitation.

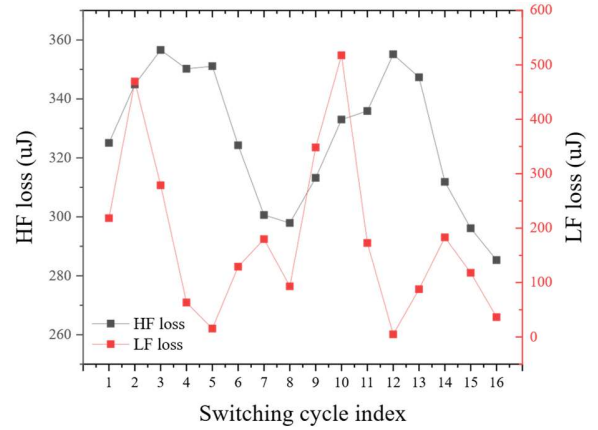


Fig. 22. High & low-frequency core loss in switching cycle level.

TABLE VI
CORE LOSS IN DIFFERENT STAGES

Loss calculation stages	Loss value (uJ)
Total loss (practical)	5637.3
Total high-frequency loss	2904.7
Low-frequency loop loss (practical)	2658.3
Low-frequency loss (after cancellation)	2614.2

VI. CONCLUSION

This paper proposes the instantaneous core loss as a fundamental concept to enable the time-domain modelling of core losses of power magnetics. The presented reactive cancellation setup provides a tool to capture the active power loss in real time that is never observed before. The existence of low-frequency core loss component in a PWM converter, which is also known as the major loop loss, is validated experimentally. Following the measurements, generic instantaneous core loss models are extracted to represent the behaviour of magnetic components as a time series. Then, a practical workflow for the cycle-by-cycle core loss estimation for the design of power magnetics in PWM DC/AC converters. This approach fills the gap of extracting the low-frequency core loss on an instantaneous basis to complete the composite

waveform hypothesis and the loss map approach. The experimental results validated the effectiveness of the method, demonstrating its accuracy across different magnetic materials. Further research following this work can be the validation with the fundamental physics-based core loss models and the thermal design for high-power industrial power electronics applications.

APPENDIX

TABLE VII
FOURIER PARAMETERS OF THE FITTED FUNCTION

a_0	0.98	w	0.61
a_1	-0.25	b_1	-0.018
a_2	0.51	b_2	0.54
a_3	0.038	b_3	-0.0438
a_4	-0.63	b_4	0.43
a_5	0.017	b_5	-0.029
a_6	-0.21	b_6	0.041

REFERENCES

- [1] J. Wang, N. Rasekh, X. Yuan and K. J. Dagan, "An Analytical Method for Fast Calculation of Inductor Operating Space for High-Frequency Core Loss Estimation in Two-Level and Three-Level PWM Converters," in *IEEE Transactions on Industry Applications*, vol. 57, no. 1, pp. 650-663, Jan.-Feb. 2021.
- [2] Seiji Iyasu, Toshihisa Shimizu, Kenichiro Ishii, A Novel Inductor Loss Calculation Method on Power Converters Based on Dynamic Minor Loop, *IEEJ Transactions on Industry Applications*, 2006, Volume 126, Issue 7, Pages 1028-1034.
- [3] J. W. Kolar et al., "PWM Converter Power Density Barriers," 2007 Power Conversion Conference - Nagoya, Nagoya, Japan, 2007, pp. P-9-P-29.
- [4] J. Muhlethaler, M. Schweizer, R. Blattmann, J. W. Kolar and A. Ecklebe, "Optimal Design of LCL Harmonic Filters for Three-Phase PFC Rectifiers," in *IEEE Transactions on Power Electronics*, vol. 28, no. 7, pp. 3114-3125, July 2013.
- [5] Jieli Li, T. Abdallah and C. R. Sullivan, "Improved calculation of core loss with nonsinusoidal waveforms," *Conference Record of the 2001 IEEE Industry Applications Conference. 36th IAS Annual Meeting (Cat. No.01CH37248)*, Chicago, IL, USA, 2001, pp. 2203-2210 vol.4.
- [6] K. Venkatachalam, C. R. Sullivan, T. Abdallah and H. Tacca, "Accurate prediction of ferrite core loss with nonsinusoidal waveforms using only Steinmetz parameters," *2002 IEEE Workshop on Computers in Power Electronics*, 2002. Proceedings., Mayaguez, PR, USA, 2002, pp. 36-4.
- [7] T. Guillod, J. S. Lee, H. Li, S. Wang, M. Chen and C. R. Sullivan, "Calculation of Ferrite Core Losses with Arbitrary Waveforms using the Composite Waveform Hypothesis," *2023 IEEE Applied Power Electronics Conference and Exposition (APEC)*, Orlando, FL, USA, 2023, pp. 1586-1593.
- [8] C. R. Sullivan, J. H. Harris and E. Herbert, "Core loss predictions for general PWM waveforms from a simplified set of measured data," *2010 Twenty-Fifth Annual IEEE Applied Power Electronics Conference and Exposition (APEC)*, Palm Springs, CA, USA, 2010, pp. 1048-1055.
- [9] S. Barg, K. Ammous, H. Mejbri and A. Ammous, "An Improved Empirical Formulation for Magnetic Core Losses Estimation Under Nonsinusoidal Induction," in *IEEE Transactions on Power Electronics*, vol. 32, no. 3, pp. 2146-2154, March 2017.
- [10] H. Matsumori, T. Shimizu, K. Takano and H. Ishii, "Evaluation of Iron Loss of AC Filter Inductor Used in Three-Phase PWM Inverters Based on an Iron Loss Analyzer," in *IEEE Transactions on Power Electronics*, vol. 31, no. 4, pp. 3080-3095, April 2016.
- [11] T. Shimizu and S. Iyasu, "A Practical Iron Loss Calculation for AC Filter Inductors Used in PWM Inverters," in *IEEE Transactions on Industrial Electronics*, vol. 56, no. 7, pp. 2600-2609, July 2009.
- [12] J. Muhlethaler, "Modeling and Multi-Objective Optimization of Inductive Power Component", Ph.D dissertation, ETH ZURICH, 2012.
- [13] A. Meng, J. Zhu, M. Kong and H. He, "Modeling of Terfenol-D Biased Minor Hysteresis Loops," in *IEEE Transactions on Magnetics*, vol. 49, no. 1, pp. 552-557, Jan. 2013.
- [14] K. Oda, K. Takano and K. Wada, "Minor Loop Position and Area Measurement of Inductors for DC-DC converter Considering Excitation Process," *2023 IEEE International Magnetic Conference - Short Papers (INTERMAG Short Papers)*, Sendai, Japan, 2023, pp. 1-2.
- [15] Yo Sakaki and T. Matsuoka, "Hysteresis losses in Mn-Zn ferrite cores," in *IEEE Transactions on Magnetics*, vol. 22, no. 5, pp. 623-625, September 1986, *Transactions on Power Electronics*, vol. 32, no. 4, pp. 2987-2994, April 2017.
- [16] C.P. Steinmetz, 1916. *Theory and calculation of alternating current phenomena* (Vol. 4). McGraw-Hill Book Company.
- [17] Akagi, H., 1983. Generalized theory of the instantaneous reactive power in three-phase circuits. In *Proc. Int. Power Electronics Conf., 1983* (pp. 1375-1386).
- [18] M. Mu, Q. Li, D. J. Gilham, F. C. Lee and K. D. T. Ngo, "New Core Loss Measurement Method for High-Frequency Magnetic Materials," in *IEEE Transactions on Power Electronics*, vol. 29, no. 8, pp. 4374-4381, Aug. 2014.
- [19] D. Hou, M. Mu, F. C. Lee and Q. Li, "New High-Frequency Core Loss Measurement Method With Partial Cancellation Concept," in *IEEE Transactions on Power Electronics*, vol. 32, no. 4, pp. 2987-2994, April 2017.
- [20] J. Wang, K. J. Dagan, X. Yuan, W. Wang and P. H. Mellor, "A Practical Approach for Core Loss Estimation of a High-Current Gapped Inductor in PWM Converters With a User-Friendly Loss Map," in *IEEE Transactions on Power Electronics*, vol. 34, no. 6, pp. 5697-5710, June 2019.
- [21] B. Cui, J. Wang, X. Yuan, J. Aguarón, A. Martínez and F. Cabaleiro, "Automated Triple Pulse Testbed (ATPT) 1.0 – Large-Signal Hardware-in-the-loop Characterization Platform for Power Magnetics," *2024 IEEE 10th International Power Electronics and Motion Control Conference (IPEMC2024-ECCE Asia)*, Chengdu, China, 2024, pp. 1613-1618.
- [22] Micrometals, "T300-26D Datasheet." <https://datasheets.micrometals.com/T300-26D-DataSheet.pdf>
- [23] J. Wang, N. Rasekh, X. Yuan and K. J. Dagan, "An Analytical Method for Fast Calculation of Inductor Operating Space for High-Frequency Core Loss Estimation in Two-Level and Three-Level PWM Converters," in *IEEE Transactions on Industry Applications*, vol. 57, no. 1, pp. 650-663, Jan.-Feb. 2021.
- [24] M. Chen et al., "MagNet Challenge for Data-Driven Power Magnetics Modeling," in *IEEE Open Journal of Power Electronics*.
- [25] D. Serrano et al., "Why MagNet: Quantifying the Complexity of Modeling Power Magnetic Material Characteristics," in *IEEE Transactions on Power Electronics*, vol. 38, no. 11, pp. 14292-14316, Nov. 2023.
- [26] S. Dulal, S. B. Sohid, H. Cui, G. Gu, D. J. Costinett and L. M. Tolbert, "A Physics-Based Circuit Model for Nonlinear Magnetic Material Characteristics," *2024 IEEE Applied Power Electronics Conference and Exposition (APEC)*, Long Beach, CA, USA, 2024, pp. 396-401.
- [27] T. Dimier and J. Biela, "Analysis of the Effect of Geometric Tolerances on Ferrite Core Losses Using a Physical Core Loss Model," *2024 Energy Conversion Congress & Expo Europe (ECCE Europe)*, Darmstadt, Germany, 2024, pp. 1-7.